

Probing the Molecular-Scale Lipid Bilayer Response to Shear Flow Using Nonequilibrium Molecular Dynamics

Philip D. Blood,^{†,‡} Gary S. Ayton,^{†,§} and Gregory A. Voth^{*,†,§}

Center for Biophysical Modeling and Simulation and Departments of Bioengineering and Chemistry, University of Utah, 315 S. 1400 E. Rm 2020, Salt Lake City, Utah 84112-0850

Received: June 7, 2005; In Final Form: August 4, 2005

A nonequilibrium molecular dynamics simulation of the response of dimyristoylphosphatidylcholine (DMPC) bilayers to a solvent shear flow is presented. Application of shear flow to planar, stationary DMPC bilayers results in a redistribution of the membrane density profile along the bilayer normal due to the alignment of the lipids in the direction of flow and an increase in average lipid chain length. An increase in the intermolecular and intramolecular order of the lipids in response to the shear flow is also observed. This study provides groundwork for understanding the mechanism of the full response of lipid bilayers to externally imposed solvent shear flows, beginning with the response in the absence of collective lipid motions such as undulations and bilayer flow.

1. Introduction

Living biological systems are constantly subjected to forces which take them away from an equilibrium state. Through mechanotransduction, these perturbations can modulate cellular function.^{1,2} Much research has been done in an effort to discover the mechanosensors and mechanisms of mechanotransduction in various systems.^{3–6} Recent studies are beginning to highlight the importance of lipid–protein interactions in mechanosensation and transduction. For example, mechanosensitive channels retain their function when reconstituted into liposomes,⁷ demonstrating that information transmitted through lipid–protein interactions alone is sufficient for gating of certain mechanosensitive channels.⁸ In addition, it was recently shown that certain toxins can inhibit mechanosensitive channels indirectly by affecting lipid–channel interactions.⁹ Another example is found in studies of shear flow on endothelial cells,¹⁰ where it is shown that fluid shear stress can activate G-proteins residing on the inner leaflet of the membrane, possibly by increasing membrane fluidity.^{11,12} This shear-induced activation is also observed when G-proteins are reconstituted into liposomes,¹³ which further demonstrates the importance of the lipid–protein interaction in mechanotransduction.

Molecular dynamics (MD) simulations can provide detailed atomistic information related to the mechanisms of these phenomena. MD simulation has already been used extensively to investigate the equilibrium properties of biologically relevant lipid bilayer systems;^{14–19} however, relatively little work has been done to characterize, in atomistic detail, the response of these lipid bilayers to nonequilibrium perturbations.

Nonequilibrium molecular dynamics (NEMD) provides a framework in which to study the lipid bilayer response to perturbations such as shear flow.^{20,21} In NEMD, Newton's equations of motion are modified to drive the system out of equilibrium. A key component of the methodology is some form

of thermostating mechanism which removes the heat generated by the nonequilibrium forces. In some cases, a “nonequilibrium steady state” may be reached.^{20,21} In the past, NEMD has been used to characterize the transport properties (e.g., shear viscosity) of various fluids, including polymers, and to connect microscopic phenomena to those predicted by classical Navier–Stokes hydrodynamics.^{20,22–25} These results are only valid inasmuch as a local thermodynamic equilibrium can be assumed.²⁶ Therefore, the general idea is to examine the system under strong fields and then perform an extrapolation to weaker fields until a linear regime is found. The zero field limit is estimated by the near zero field extrapolation. Thus, this methodology also allows one to assess the effect of perturbation strength on the behavior of the system.

The intent of this study is to characterize the response of hydrated dimyristoylphosphatidylcholine (DMPC) bilayers to hydrodynamic shear flow using NEMD. As with all NEMD simulations, the perturbation must be rather strong in order to achieve a reasonable signal-to-noise ratio. This study differs from traditional NEMD studies which are designed to investigate fluid transport. In most NEMD simulations of fluid flow, the system is reasonably homogeneous, whereas this system, by virtue of its complex molecular structure, is decidedly inhomogeneous. In other studies a synthetic wall or pore has been employed to provide the stationary reference frame and “container” for the flow²² or to model a simplified biological membrane channel.²⁷ These channel walls usually have been modeled with simplified molecular-level structures (e.g., a harmonic network of tethered springs), although water transport through a fully atomistic membrane channel has been studied.²⁸ Furthermore, the focus of previous studies was generally on the behavior of the fluid moving through the channel or the details of the emerging flow profile. However, in this study the focus is on something else, namely, the response of the membrane to the flow. Nonequilibrium molecular dynamics (NEMD) provides a framework in which to study the lipid bilayer response to perturbations such as shear flow, allowing us to directly simulate and examine individual lipid and entire membrane structural and dynamical changes.

* To whom correspondence should be addressed. E-mail: voth@chemistry.utah.edu.

[†] Center for Biophysical Modeling and Simulation.

[‡] Department of Bioengineering.

[§] Department of Chemistry.

It should be noted that a similar, and complementary, study of a coarse-grained (CG) amphiphilic bilayer under homogeneous shear was recently reported.²⁹ In this study, Lees–Edwards boundary conditions,²⁶ typically employed to calculate, for example, the nonequilibrium shear viscosity for an isotropic fluid, were employed to induce a “quasi” homogeneous shear in a CG bilayer. The shear was imposed in various directions, reflecting the symmetry of the bilayer system. In contrast, the present study seeks to examine the short time response of a bilayer to an external solvent flow where the flow is directly applied to only one leaflet of the bilayer (as in a cell or vesicle subjected to a solvent shear flow). Under periodic boundaries, this particular scenario is most easily handled using two bilayers separated by two water channels. In this way, one channel becomes a flow channel and the other one becomes a “heat reservoir” with no flow. In addition, the use of a planar, stationary lipid bilayer allows for the investigation of the membrane response to the imposed external flow in the absence of bilayer flow or undulations. Details regarding the computational nuances associated with this particular flow system can be found in section 2. Since the focus in this study is to elucidate molecular-scale mechanisms of shear-induced lipid bilayer responses, the present study employs fully atomistic (rather than CG) model resolution.

2. NEMD Simulation

Consider the scenario of two bilayers in the x – y plane separated initially by a distance h . Under periodic boundaries, this results in two distinct planar channels between the two bilayers: a central channel (W_1) and an outer channel (W_2). Each surface of the bilayers is fully hydrated. In Figure 1a, a snapshot of the initial setup is shown. We will refer to the bilayer leaflets next to the central channel as the “near” leaflets and the other two as the “far” leaflets. If we consider the positive z direction to be up, then the leaflets may be designated as upper far (UF), upper near (UN), lower near (LN), or lower far (LF). The reason for designating each leaflet separately will become apparent shortly.

At $t = 0$ (where t is the time), an external field in the x direction is applied to all of the water molecules in the *central* channel. At long enough times, a steady-state flow profile is reached. In terms of NEMD simulation, this situation can be described via a Hamiltonian

$$H(\mathbf{r}(t), \mathbf{p}(t)) = \sum_{i=1}^N \frac{|\mathbf{p}_i(t)|^2}{2m_i} + V(\mathbf{r}(t)) \quad (1)$$

where $N = N_{W_1} + N_{W_2} + N_{UF} + N_{UN} + N_{LN} + N_{LF}$ is the total number of atoms in the system. Also, $\mathbf{r}(t) = \{\mathbf{r}_1(t), \mathbf{r}_2(t), \mathbf{r}_3(t), \dots, \mathbf{r}_N(t)\}$ and $\mathbf{p}(t) = \{\mathbf{p}_1(t), \mathbf{p}_2(t), \mathbf{p}_3(t), \dots, \mathbf{p}_N(t)\}$, where $\mathbf{r}_i(t)$ is the position of atom or molecule i and $\mathbf{p}_i(t)$ is the corresponding momentum.

Before the external field is applied, the system evolves under isothermal (constant NVT) conditions. After $t = 0$, the external field, $F_{\text{ext}}\hat{\mathbf{i}}$, is applied. The equations of motion for the entire system are thus

$$\dot{\mathbf{r}}_i = \frac{\mathbf{p}_i}{m_i} \quad (2)$$

$$\dot{\mathbf{p}}_i = \mathbf{F}_i + F_{\text{ext}}g_i^{(1)}\hat{\mathbf{i}} - \xi(\mathbf{p}_i - \mathbf{p}_0)g_i^{(2)} - \sum_{k=1}^5 \alpha_k m_i g_i^{(k+1)}\hat{\mathbf{i}} \quad (3)$$

where m_i is the particle mass. The additional terms containing ξ and α will be described in detail shortly. Furthermore, $\{g_i^{(k)}\}$ are switching functions that have the property

$$g_i^{(1)} = \begin{cases} 1 & \text{for } i \in N_{W_1} \\ 0 & \text{otherwise} \end{cases} \quad (4)$$

$$g_i^{(2)} = \begin{cases} 1 & \text{for } i \in N_{W_2} \\ 0 & \text{otherwise} \end{cases}$$

$$g_i^{(3)} = \begin{cases} 1 & \text{for } i \in N_{UF} \\ 0 & \text{otherwise} \end{cases}$$

$$g_i^{(4)} = \begin{cases} 1 & \text{for } i \in N_{LN} \\ 0 & \text{otherwise} \end{cases}$$

$$g_i^{(5)} = \begin{cases} 1 & \text{for } i \in N_{LF} \\ 0 & \text{otherwise} \end{cases}$$

$$g_i^{(6)} = \begin{cases} 1 & \text{for } i \in N_{UN} \\ 0 & \text{otherwise} \end{cases}$$

In this way, distinct sets of molecules are subjected to various NEMD fields. Those molecules with $g_i^{(1)} = 1$ (i.e., the central channel waters) will experience the flow-inducing external field. Viscous heat produced in the central channel²¹ moves through the bilayers and is eventually absorbed by those water molecules with $g_i^{(2)} = 1$ (i.e., the outer channel waters). The heat is removed via a Nosé–Hoover thermostat^{30,31} that acts only on these water molecules. To ensure that the entire system is not dragged along with the flow, those molecules with $g_i^{(k)} = 1$ for $k = 2, 3, 4, 5$, and 6 (the outer channel waters and all bilayer leaflets) are subjected to a “momentum-stat”: a force that on average opposes the force due to flow, thus causing the average momentum of these subsections to be zero.

The physical picture of this scenario corresponds to a membrane that has been suspended between barriers, similar to a black membrane experiment.^{32,33} The barrier inhibits the movement of the bilayer in the presence of the shear flow. In addition, the length of the MD cell precludes any long wavelength undulations from existing in the MD system. Thus, this simulation specifically probes the response of the lipid bilayer to flow in the absence of these collective lipid motions. The momentum-stat and the thermostat employed to generate this scenario will now be discussed in greater detail.

2.1. Momentum-Statting Method. The α_k terms in the equations of motion act as momentum-stats that isolate the flow within the central channel. The form of α_k is derived from Gauss’ principle of least constraint.²⁶ The equations of motion for each α_k are

$$\dot{\alpha}_k = \frac{1}{Q_M} \sum_{i=1}^N p_i g_i^{(k+1)} \quad (5)$$

where Q_M is a constant that adjusts the strength of coupling of the momentum-stat to the system. The form of α_k is chosen to provide integral feedback that constrains the average momentum to be zero while allowing the instantaneous momentum to fluctuate around the average. Each leaflet of the bilayer is momentum-stated separately to avoid a scenario in which the leaflets within a bilayer move in opposite directions to obtain a net zero momentum.

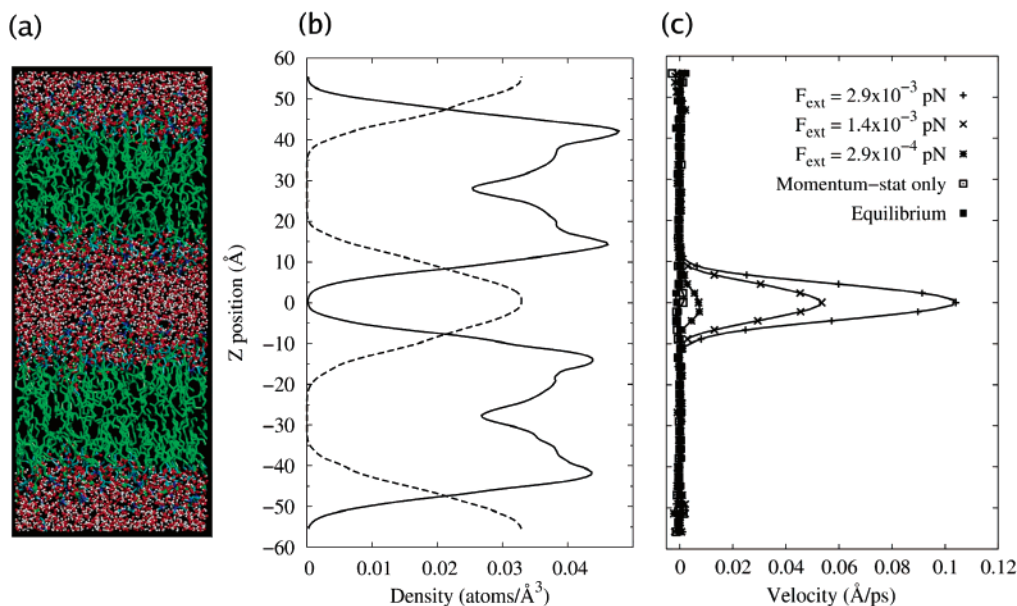


Figure 1. (a) Snapshot of the dual DMPC bilayer system. (b) Membrane (solid line) and water (dashed line) density profiles. (c) Flow profiles for various applied external fields.

2.2. Thermostating Method. Normally, when thermostating a system with flow, we would need to isolate the streaming velocities of the particles from their thermal motion (peculiar velocities) and only thermostat the latter. Failure to do so would eventually cause the formation of an artificial “string phase” and could freeze the system.³⁴ One way to address this is to design a thermostat that can distinguish between the peculiar and streaming components of the total velocity and only act on the former. This can be accomplished if there is a steady-state velocity profile that is known a priori, or if the profile can be accurately determined on the fly, or if the “flow” is simply a long wavelength motion of some section of the system.^{26,34} The first two scenarios are generally not feasible for complex molecular systems, but the third scenario may be addressed by using a profile-unbiased thermostat.²⁶ Furthermore, when shearing inhomogeneous systems, such as bilayers, local “hot spots” may develop, and the use of a global thermostat as employed in the isotropic case may then result in thermostating-induced artifacts.²⁶ Hence, the methodology for directly thermostating more complex flow scenarios in inhomogeneous systems is a topic of current research.³⁵

To address these issues in this system, the flow is isolated to the central channel and the thermostat is placed far away from the flow (N_{W_2} waters). Since the momentum-stat works via integral feedback, it may allow for long wavelength oscillatory motion of the membrane leaflets and N_{W_2} waters. To ensure that these long wavelength motions are not interpreted as heat, the thermostated particles employ a profile-unbiased thermostat where the local peculiar velocity component is resolved. This is done by defining

$$\mathbf{p}_0 = \sum_{i=1}^N \frac{\mathbf{p}_i}{N_{W_2}} g_i^{(2)}, \quad (6)$$

which isolates, for the purposes of thermostating, the nonzero total momentum of the N_{W_2} subsection. Also, an instantaneous

temperature is defined for the N_{W_2} waters such that

$$T_{k_{W_2}} = \sum_{i=1}^N \frac{|\mathbf{p}_i - \mathbf{p}_0|^2}{dm_i k_B} g_i^{(2)} \quad (7)$$

where k_B is Boltzmann’s constant and d is the number of degrees of freedom. In this case, where the thermostat acts on a subsection of the entire system in its local hydrodynamic reference frame, $d = 3(N_{W_2} - (N_{W_2} - 1)(N - 1))$. In practice, this reduces to simply $d = 3N_{W_2}$ if N_{W_2} is sufficiently large. Finally, the equation of motion for the thermostat multiplier ξ is given by

$$\dot{\xi} = \frac{1}{Q_T} (T_{k_{W_2}} - T_0) \quad (8)$$

where Q_T is the thermal inertia parameter and T_0 is the target temperature.

3. General Simulation Details

All NEMD simulations were performed using a modified version of the DL_POLY³⁶ simulation package version 2.13. Fully solvated DMPC bilayers were simulated using a united atom force field for DMPC³⁷ and the rigid TIP3P³⁸ model for water. Each bilayer consisted of 64 lipid molecules for a total of 128 lipids in the system. These were solvated by 2624 water molecules giving approximately 20.5 waters per lipid. Periodic boundary conditions were used in each Cartesian direction. All bonds were constrained using the SHAKE algorithm with a tolerance of 10^{-8} . Electrostatic interactions were calculated via a smooth particle mesh Ewald³⁹ with a tolerance of 10^{-6} . Both the real space Ewald⁴⁰ and the van der Waals interaction were cut off at 10 Å. The thermostated regions were maintained at 308 K via the Nosé–Hoover thermostat with a relaxation time of 0.2 ps. The MD time step was 0.002 ps. An initial configuration was taken from simulations of a single bilayer with 64 lipids in 1312 waters that had first been equilibrated in the NPT ensemble to obtain a stable area per lipid. Two periodic images of this configuration were stacked in the direction normal

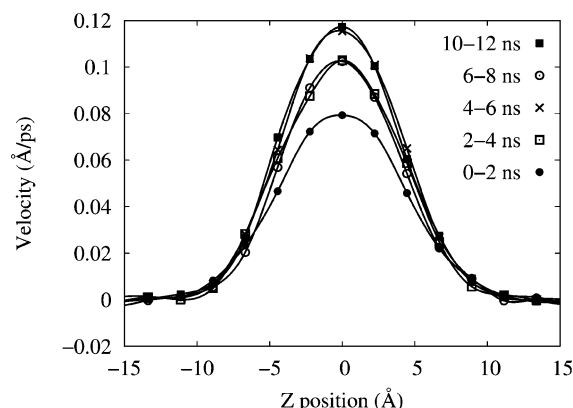


Figure 2. Channel flow profile for the strongest external field (see Figure 1c) at various times during the simulation. Flow profiles are averaged over 2 ns blocks. Lines are smooth interpolations of the data points.

to the bilayer plane (z direction) to yield the final two bilayer system. The final cell dimensions, L_x , L_y , L_z , were ~ 46.50 , ~ 41.65 , and ~ 111.47 Å, respectively. Initial configurations for flow experiments were taken after 2 ns of further equilibration in the constant NVT ensemble. Various systems with and without flow were then run for 12 ns, with averages being calculated from the last 6 ns of each run unless otherwise indicated.

4. Results

The response of DMPC lipid bilayers to a solvent shear flow was investigated using NEMD. Figure 1 shows a snapshot of the system aligned with its density profile and various velocity profiles. The momentum-stat causes each section of the system except the flow channel to have an average momentum of zero. The external force on the flow channel waters causes the velocity profile to develop. In this system it is difficult to determine when or if a fully developed flow profile will form. This is because the lipid bilayer “wall” responds to the flow over time. The flow profile develops rapidly for the highest flow and then seems to begin oscillating around a fixed value. This effect is shown in Figure 2, where the different curves correspond to the flow profile sampled at different times. Although the flow profile does not continue to grow, it is not clear that a true steady state is achieved over the time scale of these simulations. The development of the flow profile from the equilibrium starting state could, in principle, be cast within the framework of the Fluctuation Theorem.⁴¹ This, and related topics, will be the focus of future work. The lowest flow is subject to large fluctuations relative to the size of the flow profile. This is manifest in Figure 1c where a slight asymmetry in the flow profile persists even when averaged over the full 12 ns simulation.

It is clear that these flow profiles do not follow the classical Navier–Stokes result for Poiseuille flow. Other NEMD studies found deviations from the expected Navier–Stokes flow profile for channel widths of about 5 molecular diameters and near normal Navier–Stokes behavior for channels that were twice as wide.²² Because of the rough, ill-defined boundary provided by the lipids, it is difficult to determine the exact width of the channel in this system. Although the system density profile in Figure 1b shows that the water density curve persists over 40 Å, the flow profile reveals that the effective width of the channel is only about 20 Å or 6 molecular diameters. On the basis of this effective width, we are clearly in a regime where deviations from Navier–Stokes behavior are to be expected. In addition, even though the effective channel is about 20 Å, lipid head-groups have a substantial presence in the channel at a width of

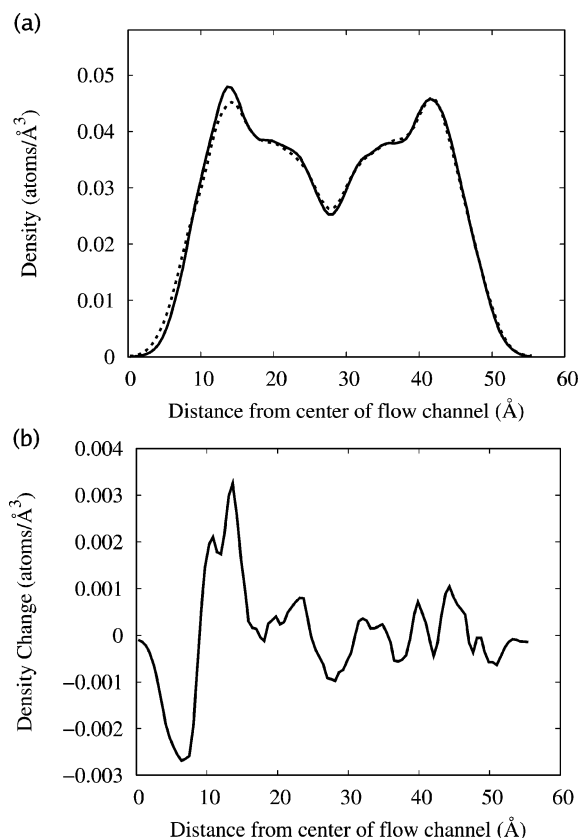


Figure 3. (a) Membrane density profiles over the course of a flow run (solid line) and an equilibrium run (dashed line). From the dual bilayer system, the single membrane density profile is obtained by averaging the two leaflets next to the flow channel together and averaging the two leaflets far from the flow channel together. The result is a single bilayer profile where one monolayer is in contact with the channel flow, while the other is in contact with the heat reservoir. (b) The difference between the two profiles in a.

only 10 Å. Thus, bulk flow behavior would only be expected in the very center of the channel with the rest of the flow occurring over the gradually transitioning boundary between water and lipid. The combination of a small effective channel width and relatively broad water–lipid boundary produces the flow profiles observed in Figure 1c.

The shear rates employed in this study, although small by NEMD standards, are of necessity much larger than those encountered in a physiological setting. The two higher shear rates result in mild heating of the system (1–2 K). The temperature does not rise throughout the course of the simulation but levels off after 2–4 ns. It would be ideal to look at a regime where no heating is observed, since this corresponds to the linear response regime and thus would theoretically allow extrapolation to a physiological level of shear. Even for the lowest shear rate, however, eventually some heating of the system is observed. In addition, the effects of flow on the membrane are difficult to discern on this time scale for all but the highest shear rate employed. Thus, the rest of the paper focuses on the results pertaining to the largest flow profile in Figure 1c.

There is a redistribution of density in the system following the application of F_{ext} at $t = 0$. Figure 3a compares the equilibrium density profile to the profile for a bilayer where one side is subjected to flow. In Figure 3b, the difference between these two profiles is plotted. An evacuation of lipids from the flow channel is observed together with denser packing at the bilayer/flow interface. There is also a slight tendency of lipids to evacuate from the center of the bilayer.

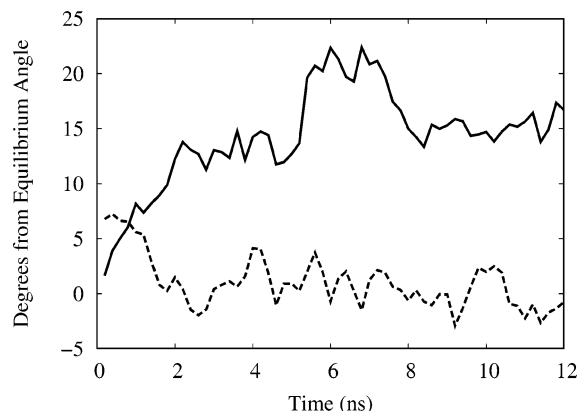


Figure 4. Degree of alignment with the direction of flow for lipids near the flow (solid line) and far from the flow (dashed line). The average equilibrium angle is taken as 0°.

These changes in the bilayer density can be explained in terms of lipid alignment with flow and lipid chain extension. Figure 4 shows the degree of alignment of the lipid molecular axis with the flow (x) direction. The average angle at equilibrium is taken as 0°. The trends in Figure 4 show strong alignment in the case of the lipids near the flow. There is a period of stronger alignment around 6 ns which then relaxes somewhat later on. Interestingly, even though there is no net flow of one leaflet over the other, the leaflets far from the flow show some tendency, albeit a weaker one, to align in the direction opposite the flow. This flow-induced alignment and molecular tilt are also observed in the CG shear study mentioned previously.²⁹

Snapshots of the leaflets near the flow are shown at different time points in Figure 5. Here the alignment of the lipids near the flow is visible to the eye. After the application of F_{ext} , the lipids near the flow become more ordered, and their chain length seems to become more uniform as they align with the flow field. The stronger alignment at 6 ns is also visible. As the lipids align with the flow, the mass of each leaflet is concentrated into a smaller region along the bilayer normal. This alignment is responsible for the increased peak heights in the density profiles.

The average chain length of the lipids is changed in the presence of the flow. Figure 6 compares the chain length response of lipids subjected to the flow (that is “turned on” at time zero) with the average chain length of the same starting configuration in the absence of the external field (i.e., equilibrium). The average chain length of the lipids near the flow quickly increases in response to the flow, while the average chain length of the lipids far from the flow follows the equilibrium system. It should be noted that longer runs would be required to sample the long wavelength modes of this collective property in both the equilibrium and nonequilibrium systems. The average chain length for the entire simulation is 13.02 ± 0.32 Å for the lipids near the flow compared to chain lengths of 12.06 ± 0.26 Å for lipids far from the flow and 12.31 ± 0.27 Å for lipids at equilibrium. This increase in average lipid chain length tends to offset the effect of lipid alignment on the density distribution. Interestingly, no change in chain length was observed in the CG shear study.²⁹ This difference may be due to bilayer movement with the flow, the shorter CG tails, or a combination of these factors.

The average chain length of lipids in a bilayer is directly related to the S_{CD} deuterium order parameter as measured by NMR. For lipids undergoing axially symmetric rotations, S_{CD}

can be calculated from computer simulations⁴² using

$$-S_{\text{CD}} = \frac{2}{3} S_{xx} + \frac{1}{3} S_{yy}, \quad (9)$$

where $S_{ii} = \langle \frac{1}{2} (3 \cos^2 \theta_{ii} - 1) \rangle$. Here θ_{ii} is the angle between the i th molecular axis of a given chain segment and the bilayer normal. This is measured for each carbon in the lipid chain.

However, in the presence of flow, lipid motion is no longer symmetric about the bilayer normal as the lipids tilt. Thus, in these simulations θ is calculated with respect to the bilayer or leaflet director. The motions of the lipids should be axially symmetric about this director. Thus, the calculated order parameter is not affected by the average tilting of the lipids.

Since the order parameter is proportional to the average chain length, it would be expected to follow the same trend in response to the flow. Figure 7 compares the order parameters for lipid chains with and without flow. The order of the chains exposed directly to flow increases not only with respect to chains far from the flow, but also with respect to the equilibrium case. The lipids far from the flow show about the same order as the equilibrium case.

This order parameter has both an intramolecular component and an intermolecular component.⁴³ The intramolecular order is related to the ratio of trans/gauche dihedrals in the lipid chains, with increasing disorder related to a greater percentage of gauche defects. Figure 8 shows the probability of gauche defects along the Sn-2 chain for lipids near the flow compared to equilibrium. There is a slight decrease in the probability of gauche defects in the presence of flow, particularly in the middle of the chain, indicating an increase in intramolecular order. Averaging the gauche probability along the entire chain yields 0.234 ± 0.006 for the lipids close to the flow vs 0.251 ± 0.005 at equilibrium.

The intermolecular order parameter is given by $S_{\text{mol}} = \langle \frac{1}{2} (3 \cos^2 \theta_{\text{inter}} - 1) \rangle$, where θ_{inter} is the angle between the long lipid axis and the director.^{43,44} The value of S_{mol} obtained for the equilibrium case is 0.709 ± 0.019 , in excellent agreement with the experimental value of 0.711.^{43,44} For lipids near the flow, the value of S_{mol} increases to 0.814 ± 0.025 . Thus, the orientational order of the lipids increases substantially in response to the flow. This result together with Figure 8 nicely explains the total increased chain order observed in Figure 7. There is increased order across the entire chain due to the increased intermolecular order, with a region of enhanced ordering in the middle of the chain due to an increased intramolecular ordering shown by a lower probability of gauche defects.

Two membrane dynamical properties which may be related to membrane fluidity were also examined: the lipid mean-square displacement (MSD) in the direction perpendicular to the flow and the trans–gauche isomerization rate of the lipid chains. However, on the time scale of these experiments, no changes in either of these quantities were observed in response to the flow.

5. Possible Relations to Experimental Observations

It is interesting to cast these results with experimental setups designed to measure membrane responses to solvent shear flow. From experimental evidence, it is postulated that external shear flow increases fluidity in membranes. One line of evidence comes from experiments with the fluorescent probe 9-(dicyanovinyl)-julolidine (DCVJ), which is sensitive to the microviscosity of the membrane, in particular, the rate of trans–gauche isomerization of the lipid chains.⁴⁵ Experiments on endothelial cells showed that DCVJ in the cell membrane

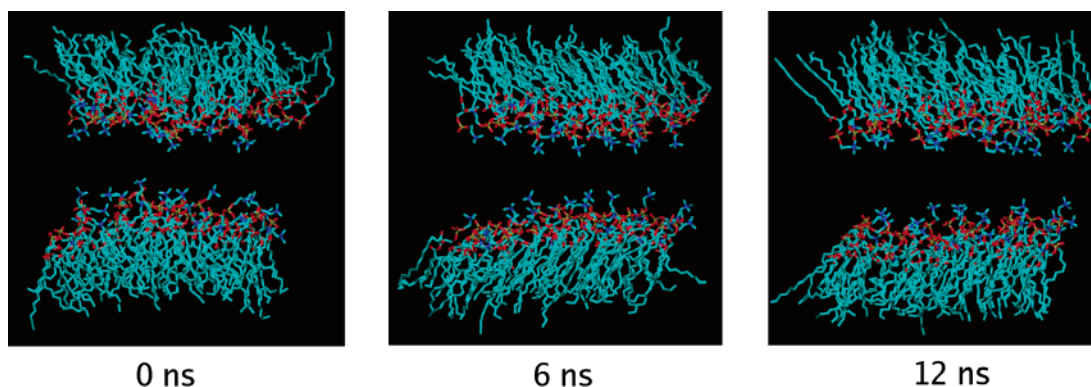


Figure 5. Snapshots of the lipids near the flow at various points in the flow simulation. Water molecules are removed from the figure to more clearly show the lipid structure.

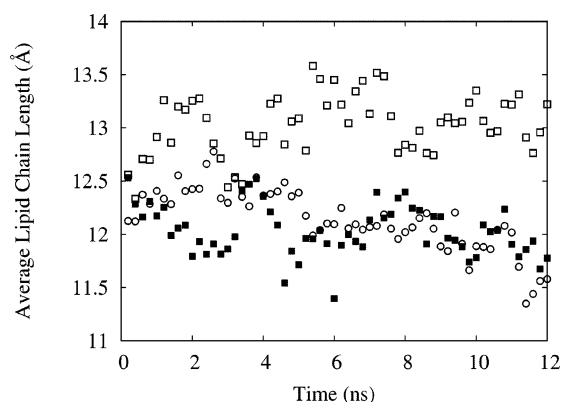


Figure 6. Average Sn-2 chain length for lipids near the flow (open squares), far from the flow (solid squares), and at equilibrium (open circles). Chain lengths are calculated as the distance between C₁ and C₁₄ carbon atoms, with 0.81 Å added to account for the C–H bond of the terminal carbon.⁴³ Data points are averages over 200 ps blocks.

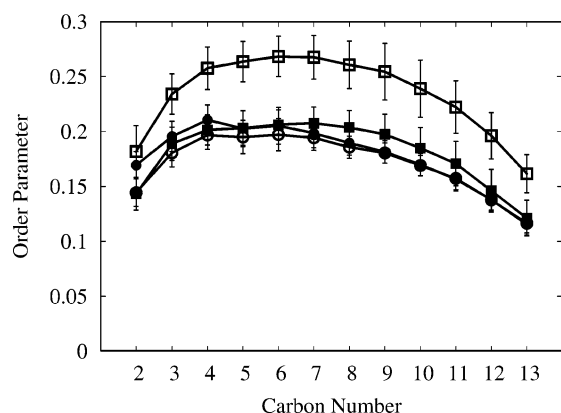


Figure 7. Order parameters for the Sn-2 chain of lipids near the flow (open squares), far from the flow (solid squares), and at equilibrium (open circles) calculated with respect to the membrane director. For the equilibrium case, the order parameter is also calculated with respect to the bilayer normal (solid circles). Error bars are determined by averaging over 200 ps blocks.

decreased its quantum yield in response to fluid shear stress, indicating an increase in membrane fluidity.¹¹ It has also been shown that application of shear flow can increase the rate of lateral lipid diffusion in cells in the direction perpendicular to the flow.^{12,46} It is hypothesized that these changes in membrane fluidity cause the observed activation of G-proteins embedded in the inner membrane leaflet in response to flow.¹³

Molecular dynamics simulations have the ability to distinguish between the various effects of flow on the membrane and shed light on the mechanism of flow modulation of lipid bilayer

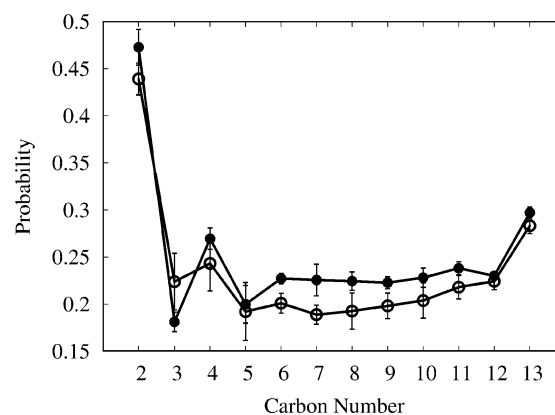


Figure 8. Probability of gauche defects along the Sn-2 chain of lipids near the flow (open circles) and at equilibrium (solid circles). Error bars are determined by averaging over 1 ns blocks.

properties. In the simulations reported here, no change in the rate of trans–gauche isomerization or lipid MSD (perpendicular to flow) is observed in response to flow. What is observed is an increase in the order of lipids subjected to external shear flow. In interpreting these results it is important to keep in mind that, while membrane fluidity (rate of molecular motion) and membrane order are often related, they are not equivalent.⁴⁷ The nature of the relationship between lipid order and the rate of lipid motions has been discussed elsewhere.^{48,49} In some cases one of these may change without the other, depending upon the particular conditions (e.g., going from a liquid-ordered to a liquid-disordered state).⁵⁰ Such was the case in these simulations in which an increase in lipid order and decrease in gauche defects were observed, but no change in the rate of lipid trans–gauche isomerization was discerned. It should be noted that the time scale of these simulations may not have been long enough to discern changes in lateral lipid translation, since the correlation times of this process are on the order of 10^{-7} s.⁴⁹ However, the correlation time of trans–gauche isomerization is around 100 ps, and hence if substantial changes occurred, then they should be discernible in these simulations. To resolve the mechanism of lipid bilayer mediated mechanotransduction, it is necessary to determine how both lipid order and rates of lipid motion are affected by flow.

It is highly likely that the increased fluidity observed in experiment is due, at least in part, to undulations and other motions that occur on longer length and time scales than those accessible by traditional MD. Indeed, this possibility is currently being investigated experimentally.⁵¹ This study supports that idea and shows that in the absence of bilayer flow and membrane undulations, the effect of an external shear flow is

to increase membrane lipid order. It would be interesting to investigate whether these increases in lipid order might result in an increased membrane bending modulus. If shear flow enhances membrane undulations,^{29,51} an increased bending modulus may provide some negative feedback that subdues large undulations and tends to stabilize the membrane in the presence of strong flows.

6. Summary

The response of planar, stationary lipid bilayers to a solvent shear flow has been studied on a multi-nanosecond time scale. Under these conditions, the effect of an external shear flow is to increase the order of the lipid bilayer. Further study is needed to determine the impact this response may have on the macroscopic behavior of these systems and the additional effects that may be seen by allowing long-wavelength collective lipid motions such as undulations. This study represents a first step in an incremental, multiscale computational and conceptual process that should provide insight into the mechanisms behind experimental observations. Multiscale simulation methodologies in development in our group^{52–57} should eventually make it viable to incorporate the full range of possible membrane responses to flow, allowing the isolation of effects due to long time- and length-scale motions.

Acknowledgment. We are grateful to Harald Tepper, Rakwo Chang, and Liam McWhirter for their insights during many helpful discussions. This research was supported by the National Institutes of Health (R01 GM63796). Computations were performed on systems located at the National Center for Supercomputing Applications and the Pittsburgh Supercomputing Center, supported by the National Science Foundation under the following NSF programs: Partnerships for Advanced Computational Infrastructure, Distributed Terascale Facility (DTF), and Terascale Extensions: Enhancements to the Extensible Terascale Facility. Some computations were also performed on resources administered by the University of Utah Center for High Performance Computing.

References and Notes

- Huang, H. D.; Kamm, R. D.; Lee, R. T. *Am. J. Physiol.: Cell Physiol.* **2004**, *287*, C1–C11.
- Gillespie, P.; Walker, R. *Nature* **2001**, *413*, 194–202.
- Davies, P. *Physiol. Rev.* **1995**, *75*, 519–560.
- Blount, P. *Neuron* **2003**, *37*, 731–734.
- Goodman, M. B.; Schwarz, E. M. *Annu. Rev. Physiol.* **2003**, *65*, 429–452.
- Martinac, B. *J. Cell Sci.* **2004**, *117*, 2449–2460.
- Sukharev, S. I.; Blount, P.; Martinac, B.; Blattner, F. R.; Kung, C. *Nature* **1994**, *368*, 265–268.
- Poolman, B. *Mol. Microbiol.* **2002**, *44*, 889–902.
- Suchyna, T. M.; Tape, S. E.; Koeppe, R. E.; Andersen, O. S.; Sachs, F.; Gottlieb, P. A. *Nature* **2004**, *430*, 235–240.
- Gudi, S. R.; Clark, C. B.; Frangos, J. A. *Circ. Res.* **1996**, *79*(4), 834–839.
- Haidekker, M. A.; L'Heureux, N.; Frangos, J. A. *Am. J. Physiol.: Heart Circ. Physiol.* **2000**, *278*, H1401–H1406.
- Butler, P. J.; Norwich, G.; Weinbaum, S.; Chien, S. *Am. J. Physiol.: Cell Physiol.* **2001**, *280*, C962–C969.
- Gudi, S.; Nolan, J. P.; Frangos, J. A. *Proc. Natl. Acad. Sci.* **1998**, *95*(5), 2515–2519.
- Pandit, S. A.; Bostick, D.; Berkowitz, M. L. *Biophys. J.* **2003**, *85*, 3120–3131.
- Hofsass, C.; Lindahl, E.; Edholm, O. *Biophys. J.* **2003**, *84*, 2192–2206.
- Khelashvili, G. A.; Scott, H. L. *J. Chem. Phys.* **2004**, *120*, 9841–9847.
- Feller, S. E.; Gawrisch, K.; MacKerell, A. D. *J. Am. Chem. Soc.* **2002**, *124*, 318–326.
- de Vries, A. H.; Mark, A. E.; Marrink, S. J. *J. Phys. Chem. B* **2004**, *108*, 2454–2463.
- Moore, P. B.; Lopez, C. F.; Klein, M. L. *Biophys. J.* **2001**, *81*, 2484–2494.
- Todd, B.; Evans, D.; Daivis, P. *Phys. Rev. E* **1995**, *52*, 1627–1638.
- Todd, B.; Daivis, P.; Evans, D. *Phys. Rev. E* **1995**, *51*, 4362–4368.
- Travis, K. P.; Todd, B. D.; Evans, D. J. *Physica A* **1997**, *240*, 315–327.
- Travis, K. P.; Todd, B. D.; Evans, D. J. *Phys. Rev. E* **1997**, *55*, 4288–4295.
- Ayton, G.; Jepps, O. G.; Evans, D. J. *Mol. Phys.* **1999**, *96*, 915–920.
- Bosko, J. T.; Todd, B. D.; Sadus, R. J. *J. Chem. Phys.* **2004**, *121*, 1091–1096.
- Evans, D. J.; Morriss, G. P. *Statistical Mechanics of Nonequilibrium Liquids*; Academic Press: London, 1990.
- Crozier, P. S.; Rowley, R. L.; Holladay, N. B.; Henderson, D.; Busath, D. D. *Phys. Rev. Lett.* **2001**, *86*, 2467–2470.
- Zhu, F. Q.; Tajkhorshid, E.; Schulten, K. *Biophys. J.* **2002**, *83*, 154–160.
- Shkulipa, S.; den Otter, W.; Briels, W. *Biophys. J.* **2005**.
- Hoover, W. G. *Phys. Rev. A* **1985**, 1695–1697.
- Evans, D.; Holian, B. J. *J. Chem. Phys.* **1985**, *83*, 4069–4074.
- Ogier, S. D.; Bushby, R. J.; Cheng, Y. L.; Evans, S. D.; Evans, S. W.; Jenkins, A. T. A.; Knowles, P. F.; Miles, R. E. *Langmuir* **2000**, *16*, 5696–5701.
- Chernyshev, A.; Armstrong, K. M.; Cukierman, S. *Biophys. J.* **2003**, *84*, 238–250.
- Evans, D.; Morriss, G. *Phys. Rev. Lett.* **1986**, *56*, 2172–2175.
- Delhommelle, J.; Petracic, J.; Evans, D. J. *J. Chem. Phys.* **2003**, *119*, 11005–11010.
- Smith, W.; Forester, T. R. *The DL_POLY molecular simulation package*, http://www.cse.clrc.ac.uk/msi/software/DL_POLY, 1999.
- Smondirev, A. M.; Berkowitz, M. L. *J. Comput. Chem.* **1999**, *20*, 531–545.
- Jorgensen, W. L.; Chandrasekhar, J.; Madura, J. D.; Impey, R. W.; Klein, M. L. *J. Chem. Phys.* **1983**, *79*, 926–935.
- Essmann, U.; Perera, L.; Berkowitz, M.; Darden, T.; Lee, H.; Pedersen, L. G. *J. Chem. Phys.* **1995**, *103*, 8577–8593.
- de Leeuw, S. W.; Perram, J. W.; Smith, E. R. *Proc. R. Soc. London* **1980**, *A373*, 26–56.
- Evans, D. J.; Searles, D. J. *Adv. Phys.* **2002**, *51*, 1529–1585.
- Egberts, E.; Berendsen, H. J. *J. Chem. Phys.* **1988**, *89*, 3718–3732.
- Douliez, J.; Léonard, A.; Dufourc, E. J. *Biophys. J.* **1995**, *68*, 1727–1739.
- Dufourc, E. J.; Mayer, C.; Stohrer, J.; Althoff, G.; Kothe, G. *Biophys. J.* **1992**, *61*, 42–57.
- Kung, C.; Reed, J. *Biochemistry* **1986**, *25*, 6114–6121.
- Butler, P. J.; Tsou, T. C.; Li, J. Y. S.; Usami, S.; Chien, S. *FASEB J.* **2002**, *16*, 216–218.
- Seelig, A.; Seelig, J. *Biochemistry* **1974**, *13*, 4839–4845.
- Yeagle, P. L. *The Membranes of Cells*, 2nd ed.; Academic Press: New York, 1993; Chapter 4.
- Gawrisch, K. In *The Structure of Biological Membranes*, 2nd ed.; Yeagle, P. L., Ed.; CRC Press: New York, 2005; Chapter 4.
- Wilson-Ashworth, H. A.; Harris, F. M.; Shinkle, A.; Erickson, J.; Jensen, L. B.; Bell, J. D. *Biophys. J.* **2004**, *86*, 31A.
- Haidekker, M. A.; Stevens, H. Y.; Frangos, J. A. *Ann. Biomed. Eng.* **2004**, *32*, 531–536.
- Ayton, G.; Bardenhagen, S. G.; McMurtry, P.; Sulsky, D.; Voth, G. A. *J. Chem. Phys.* **2001**, *114*, 6913–6924.
- Ayton, G.; Smondirev, A. M.; Bardenhagen, S. G.; McMurtry, P.; Voth, G. A. *Biophys. J.* **2002**, *83*, 1026–1038.
- Ayton, G.; Voth, G. A. *Biophys. J.* **2002**, *83*, 3357–3370.
- Ayton, G. S.; Tepper, H. L.; Mirijanian, D. T.; Voth, G. A. *J. Chem. Phys.* **2004**, *120*, 4074–4088.
- Ayton, G.; Voth, G. A. *Biophys. J.* **2004**, *87*, 3299–3311.
- Chang, R.; Ayton, G.; Voth, G. A. *J. Chem. Phys.* **2005**.